SMC-TR-00-30

AEROSPACE REPORT NO.
TR-2000(8570)-4

Multiple Discrete-Energy Ion Features in the Inner Magnetosphere: Observations and Simulations

August 2000

Prepared by

XINLIN LI,[1] D. N. BAKER,[2] M. TEMERIN,[3] W. K. PETERSON,[4]

and

J. F. FENNELL
Laboratory Operations
Engineering and Technology Group

Prepared for

SPACE AND MISSILE SYSTEMS CENTER
AIR FORCE MATERIEL COMMAND
2430 E. El Segundo Boulevard
Los Angeles Air Force Base, CA 90245

Contract No. F04701-93-C-0094

Engineering and Technology Group

[1] LASP, University of Colorado, Boulder, CO
[2] LASP, University of Colorado, Boulder, CO
[3] Space Sciences Lab., University of California, Berkeley, CA
[4] Lockheed Martin, Palo Alto, CA

THE AEROSPACE CORPORATION
El Segundo, California

This report was submitted by The Aerospace Corporation, El Segundo, CA 90245-4691, under Contract No. F04701-93-C-0094 with the Space and Missile Systems Center, Air Force Materiel Command, 2430 E. El Segundo Blvd., Los Angeles Air Force Base, CA 90245. It was reviewed and approved for The Aerospace Corporation by L. T. Greenberg, Vice President, Technology Operations. Mr. Michael Zambrana was the project officer for the Mission-Oriented Investigation and Experimentation (MOIE) program.

This report has been reviewed by the Public Affairs Office (PAS) and is releasable to the National Technical Information Service (NTIS). At NTIS, it will be available to the general public, including foreign nations.

This technical report has been reviewed and is approved for publication. Publication of this report does not constitute Air Force approval of the report's findings or conclusions. It is published only for the exchange and stimulation of ideas.

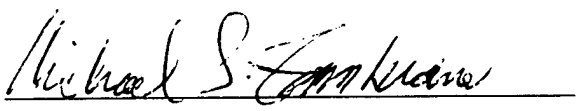

MR. MICHAEL ZAMBRANA
MOIE Project Officer

REPORT DOCUMENTATION PAGE

Form Approved
OMB No. 0704-0188

1. AGENCY USE ONLY (Leave blank)	2. REPORT DATE	3. REPORT TYPE AND DATES COVERED
	August 2000	

4. TITLE AND SUBTITLE

Multiple Discrete-Energy Ion Features in the Inner Magnetosphere: Observations and Simulations

5. FUNDING NUMBERS

F04701-93-C-0094

6. AUTHOR(S)

Xinlin Li, D. N. Baker, M. Temerin, W. K. Peterson, and J. F. Fennell

7. PERFORMING ORGANIZATION NAME(S) AND ADDRESS(ES)

The Aerospace Corporation
Technology Operations
El Segundo, CA 90245-4691

8. PERFORMING ORGANIZATION REPORT NUMBER

TR-2000(8570)-4

9. SPONSORING/MONITORING AGENCY NAME(S) AND ADDRESS(ES)

Space and Missile Systems Center
Los Angeles Air Force Base, CA 90245

10. SPONSORING/MONITORING AGENCY REPORT NUMBER

SMC-TR-00-30

11. SUPPLEMENTARY NOTES

12a. DISTRIBUTION/AVAILABILITY STATEMENT

Approved for public release; distribution unlimited

12b. DISTRIBUTION CODE

13. ABSTRACT (Maximum 200 words)

Recent measurements from the ion composition sensors (CAMMICE/MICS and TIMAS) on the Polar satellite often show multiple discrete-energy peaks in ion-energy spectra, which are seen as multiple bands in energy-time plots. The most striking feature is that these multiple bands occur over a large range of L (L=3–8) and energy (a few keV to hundreds of keV) independent of the mass of the ions. These events are more likely to be observed during quiet times following substorm activity. Using an event observed on Feb. 9, 1998 we interpret the observed ion bands as the result of a time-of-flight effect of the particle's drift around the Earth. We demonstrate by test-particle simulations that these multiple bands across a large range of L and energy are ion drift echoes that can be injected into the inner magnetosphere from the plasmasheet by a single earthward propagating time-varying field associated with substorm dipolarization. The existence of ion drift echoes even after only moderate substorm activity shows that localized time-varying electric and magnetic fields such as modeled here can and do penetrate deep into the inner magnetosphere.

14. SUBJECT TERMS

15. NUMBER OF PAGES
4

16. PRICE CODE

17. SECURITY CLASSIFICATION OF REPORT	18. SECURITY CLASSIFICATION OF THIS PAGE	19. SECURITY CLASSIFICATION OF ABSTRACT	20. LIMITATION OF ABSTRACT
Unclassified	Unclassified	Unclassified	

Abstract. Recent measurements from the ion composition sensors (CAMMICE/MICS and TIMAS) on the Polar satellite often show multiple discrete-energy peaks in ion-energy spectra, which are seen as multiple bands in energy-time plots. The most striking feature is that these multiple bands occur over a large range of L (L=3–8) and energy (a few keV to hundreds of keV) independent of the mass of the ions. These events are more likely to be observed during quiet times following substorm activity. Using an event observed on Feb. 9, 1998 we interpret the observed ion bands as the result of a time-of-flight effect of the particle's drift around the Earth. We demonstrate by test-particle simulations that these multiple bands across a large range of L and energy are ion drift echoes that can be injected into the inner magnetosphere from the plasmasheet by a single earthward propagating time-varying field associated with substorm dipolarization. The existence of ion drift echoes even after only moderate substorm activity shows that localized time-varying electric and magnetic fields such as modeled here can and do penetrate deep into the inner magnetosphere.

Introduction

Energetic particle injection into the inner magnetosphere is an intrinsic process of magnetospheric substorms [McIlwain, 1974; Ejiri et al., 1980; Moore et al., 1981; Mauk and Meng, 1987; Birn et al., 1997]. Here, we focus on a particular feature of energetic ions (a few keV to hundreds of keV) in the inner magnetosphere, namely, multiple discrete-energy bands. Such features have long been observed at geosynchronous orbit [e.g., Mauk and Meng, 1983; Grande et al., 1992] and are likely a consequence of drift echoes of different energy ions [Grande et al., 1992]. However, recent measurements from the ion composition sensors on the Polar satellite often show such multiple peaks in energy spectra over a large range of L (L=3–8) and energy (a few keV to hundreds of keV) independent of the mass and charge of the ions. These events are more likely to be observed during quiet times following substorm activity based on about 16 months of Polar data taken from Nov. 1996 through April 1998 [Fennell et al., 1998].

Observations

The Polar satellite was launched in Feb. 1996 with an inclination of 86°, an apogee of $9R_E$, and a perigee of $1.8R_E$. It traverses the inner magnetosphere twice per orbit (17.5 hours). Fig. 1 shows spectrograms obtained from two ion composition sensors on Polar, the MICS sensor of the Charge and Mass Magnetospheric Ion Composition Experiment (CAMMICE) [Wilken et al., 1992] and the Toroidal Imaging Mass-Angle Spectrographs (TIMAS) [Shelley et al., 1995]. The first three panels display color-coded differential fluxes of different ion species as energy vs. time from CAMMICE/MICS, the 4th panel displays the total-ion pitch angle distribution for the energy range of 6-80 keV. The last two panels display color-coded differential fluxes of different ions from TIMAS. Note:

(1)The multiple-band features (multiple maxima and minima in the flux) are evident across a wide range of L and energy independent of the mass of the ions. Though expected, it is nice to see that in the energy overlap region, 1 keV-30 keV, MICS and TIMAS sensors show the same result. The energy spectrum for ions with energy greater than 10 keV in the magnetosphere can usually be described as a kappa-like or a power law distribution. Obviously these multiple-band features cannot be described by any such monotonic energy spectrum.

(2)The pitch angle distribution as shown in 4th panel is almost gyrotropic as is evident from the symmetry between 0°-180° and 180°-360° fluxes and relatively isotropic except for a loss cone feature and a slight peak at 90° through out the inner magnetosphere traverse.

(3)The magnetosphere was very quiet for many hours prior to the interval shown in Fig. 1 and there was no sign of magnetic storm activity for the previous five days (Dst remained above -23nT). Kp was below 3 and AE remained below 50 nT for longer than six hours prior to the observation [Website of Kyoto University, Japan].

The above event on Feb. 9, 1998 and other similar events such as on Sept. 3, 1997, which also occurred during a quiet time following a substorm, have been discussed [Fennell et al., 1998; Peterson et al., 1998] but have not been interpreted in terms of particle drift echoes. Here for the first time, we interpret this feature as a result of time-of-flight effects on an ion's drift around the Earth, and also for the first time demonstrate by test-particle simulations that these multiple bands, spanning a large range of L and energy, are ion drift echoes that can be caused by a single injection that is the result of a single fluctuation in the electric and magnetic fields.

Model

Our field model is identical to that used to simulate dispersionless injections (particles with different energies that enhance simultaneously) and subsequent drift echoes of energetic electrons and protons observed at geosynchronous orbit [Li et al., 1998, 1999]. This model was modified from one originally developed to model the sudden compression of the magnetosphere by a strong interplanetary shock [Li et al., 1993].

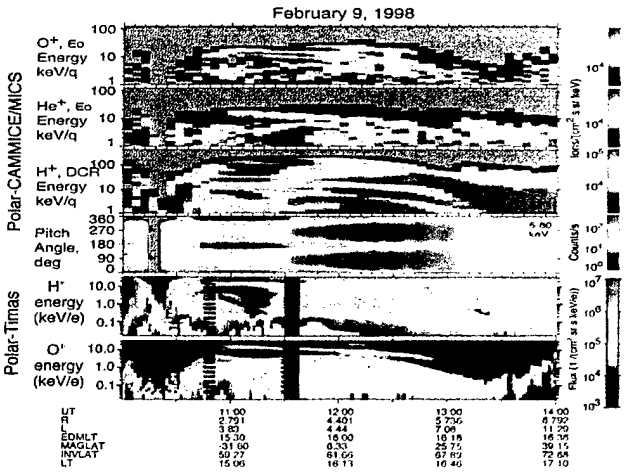

Figure 1. POLAR/CAMMICE/MICS and TIMAS measurements for 1000-1400 UT on February 9, 1998.

The modeled time-varying fields can be associated with a dipolarization, during which the northward magnetic field in the magnetic equatorial plane increases due to a temporally and spatially varying westward-pointing electric field. The modeled perturbed fields propagate earthward from the magnetotail. The electric field is a time-dependent Gaussian pulse with a purely azimuthal electric field component with a half-width of 3.48 R_E propagating radially inward at a constant velocity of 100 km/s. The modeled electric field decreases away from midnight with a maximum amplitude of 4mV/m at midnight and 0.5mV/m at dawn and dusk, and is partially reflected at the plasmapause, which is assumed at $3.5R_E$. The time-varying magnetic field is determined from Faraday's law. The variation occurs first at local midnight and subsequently at other longitudes.

We superimposed this time-varying field on the background magnetic field, which is asymmetric. At geosynchronous orbit, e.g., it has a magnetic field strength of 105 nT at local noon, 75 nT at midnight, and 90 nT at dawn and dusk, which is comparable to average magnetic field measurements [Li et al., 1998]. Our field model implicitly contains many of the effects often mentioned in the description of substorm onsets, as discussed in [Li et al., 1998].

We followed protons using a guiding center approximation, for $v_{\parallel} = 0$, [Northrop, 1963]

$$\dot{W} = q\dot{\mathbf{R}}_{\perp} \cdot \mathbf{E}_w + \frac{M_r}{\gamma}\frac{\partial B}{\partial t}, \tag{1}$$

$$\dot{\mathbf{R}}_{\perp} = \frac{\hat{e}_{\perp}}{B} \times (-c\mathbf{E}_w + \frac{M_r c}{\gamma q} \bigtriangledown B), \tag{2}$$

where $\dot{\mathbf{R}}_{\perp}$ describes the guiding center motion perpendicular to the instantaneous magnetic field $\mathbf{B} = \mathbf{B}_E + \mathbf{B}_w$, $\hat{e}_{\perp} = \mathbf{B}/B$ is a unit vector along $\mathbf{B}$, $\gamma = (W + m_0c^2)/m_0c^2$ is the relativistic energy factor, W is the particle's kinetic energy, $M_r = p_{\perp}^2/2m_0B$ is the relativistic adiabatic invariant and $p_{\perp}$ is the particle's perpendicular momentum.

We followed 567,648 protons in the combined pulse and background fields. The protons were initially distributed in the equatorial plane at distances from r=3.5–18R_E in increments of $0.1R_E$, in azimuth every 5°, and at energies between 0.5 and 203 keV in increments of 1.12%. All pro-

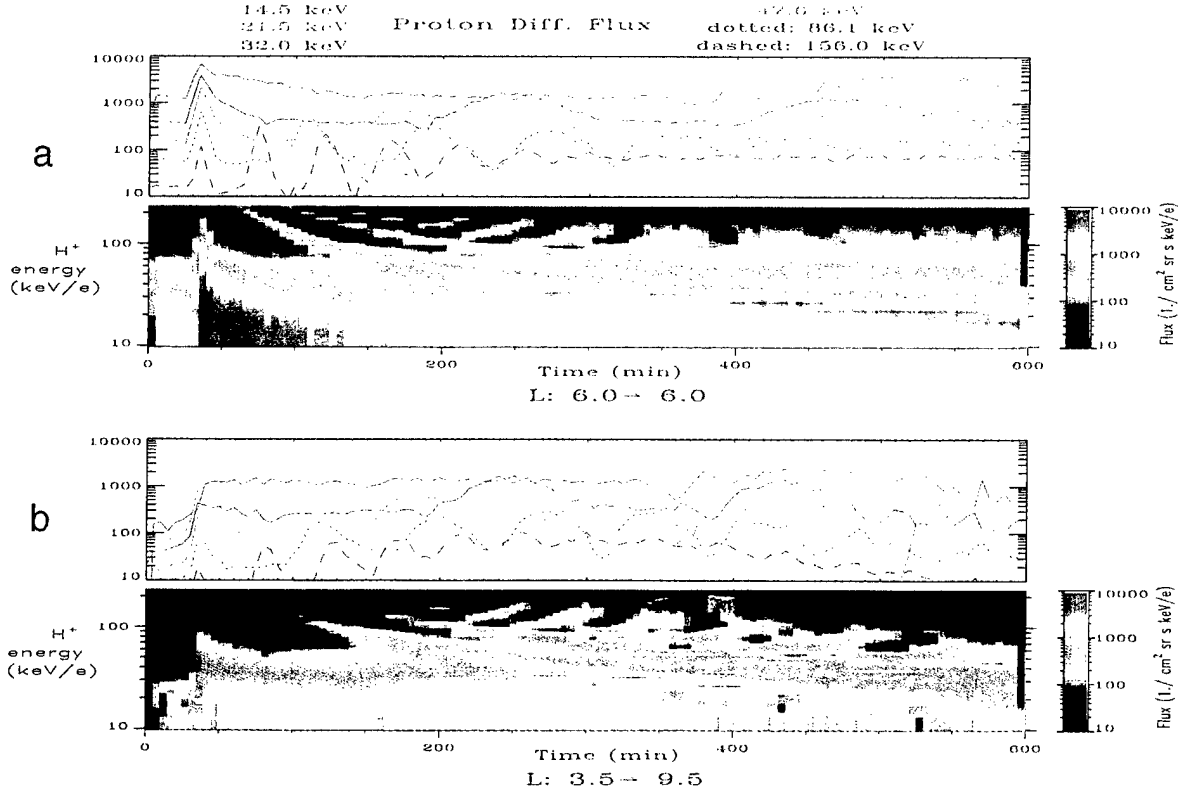

Figure 2. (a) Top panel is a line plot for selected energy channels as labeled. The bottom panel is an energy spectrum plot of the same simulation but with many more energy channels. The virtual s/c stays at 6 R_E at local midnight. (b) same as (a) except the virtual s/c moves from 3.5 R_E to 9.5 R_E at a constant speed, $V_s/_c$=0.01 R_E/min.

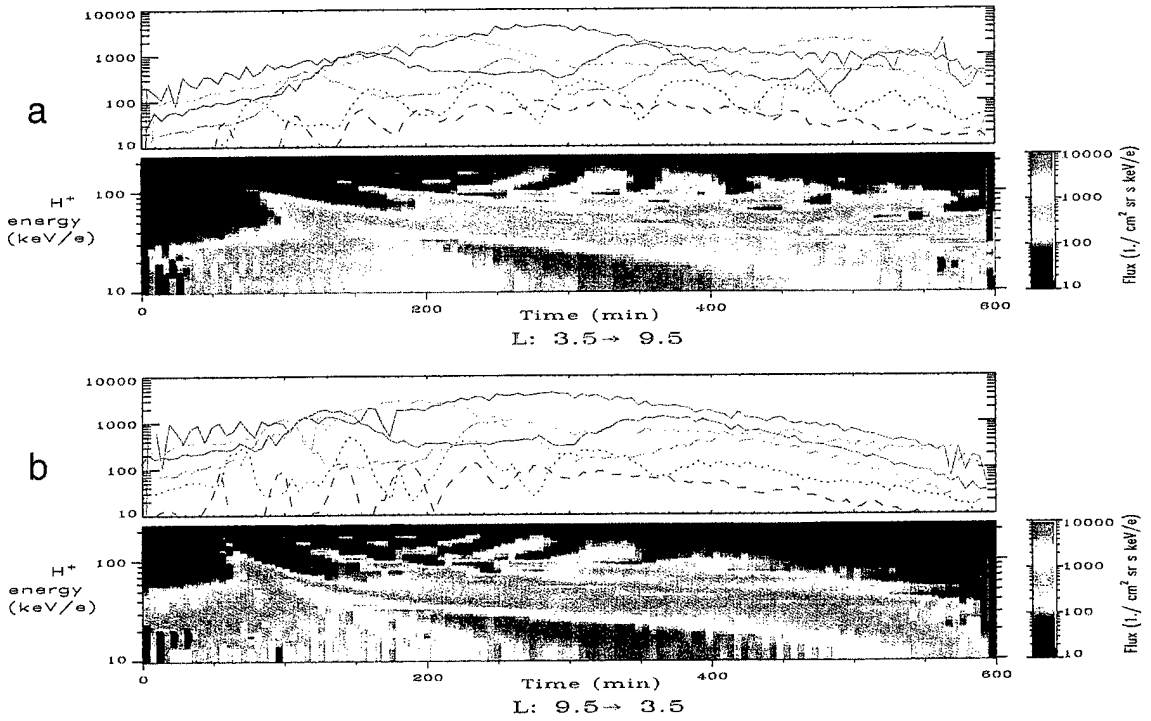

Figure 3. (a) same as Figure 2a except the virtual s/c moves from 3.5 R_E to 9.5 R_E at local noon at the same constant speed. (b) same as Figure 3a except the virtual s/c moves from 9.5 R_E to 3.5 R_E at the same constant speed.

tons had 90° pitch angles. In the post-processing stage each proton was given a weight which depended on the assumed initial distribution in energy and radial distance [Li et al., 1993]. The initial energy distribution was a kappa distribution [Vasyliunas, 1968] with $\kappa = 3$ and $E_0 = 2.5$ keV. These parameters are typical for a moderately active plasma sheet [Christon et al., 1991]. The initial radial dependence, f, was given by

$$f = [\frac{(r_0 - a_0)^{nl}}{r_0^{ml}}]/[\frac{(a_{0d} - a_0)^{nl}}{a_{0d}^{ml}}], \qquad (3)$$

where r_0 is the initial radial distance of the particle, and $a_0 = 3.3, nl = 5, ml = 12, a_{0d} = 6$. Thus, given an initial proton distribution, we can obtain proton fluxes and distributions at any location and time and can compare the simulation results with the observations. The fluxes were summed over $\pm 1 R_E$ with a time resolution of 5 minutes. There are no new injections and no loss in the simulation.

Results

Figure 2a shows an example of our simulation results at r=6R_E at midnight. The top panel shows differential fluxes of protons for selected energy channels as labeled. The bottom panel is an energy spectrogram plot of the same simulation but with all > 10 keV TIMAS channels, which measure up to 33 keV/q, and with extrapolated higher energy channels. The TIMAS instrument response has been incorporated in the spectral plot and extrapolated to higher energies. The satellite first measures an almost simultaneous enhancement of protons of all energies because the dipolarization starts at midnight. The dipolarization starts far from Earth (> 18R_E) and transports particles earthward. The physical processes involved in dispersionless injection have been discussed in Li et al. [1998]. From the line plot (top panel) and equation (2), it is evident that injected particles drift around the Earth because of the gradient of the magnetic field. Since energetic protons drift faster, they can overlap lower energy protons and for a given time can have higher fluxes: this is simply a time-of-flight effect. The multiple bands are evident when the energy spectrum (bottom panel) is plotted as color-coded flux level. It should be noted that the clump-like features in the energy spectrum plot (upper end) are simply due to poor statistics in the simulation.

Figure 2b shows the result if the virtual satellite at midnight moves from 3.5R_E to 9.5R_E at a constant speed, demonstrating that the multiple bands can exist for a wide range of radial distance and time.

Figures 3a and 3b show the same simulation but with the virtual satellite at noon moving from 3.5R_E to 9.5R_E and vice versa. Since the satellite is far away from the injection site (midnight), it measures a dispersed injection, more energetic particles reach the satellite first because they drift faster. The most energetic protons drift around the Earth a few times before the injected low energy protons reach the satellite.

Discussions

Observations and Simulations

Since we consider only equatorially mirroring particles and our virtual satellites stays in the equatorial plane, we do not attempt to actually reproduce the observation shown in Fig. 1 . Furthermore our model does not include the convection and corotation electric fields. However, the simulation results demonstrate that multiple discrete energy ion features can be a manifestation of drift echoes of suddenly injected particles. The following points help to show the association of the simulation results with actual observations.

Simple model and variety of structures Simulation results presented here are from only one set of model

parameters. All the differences shown in Figs. 2 and 3 are due to the location and motion of the virtual satellite. This shows that different satellite traversing the inner magnetosphere can measure different ion features depending on the relative timing and location of the satellite with respect to the particle injection. For example, the equatorial crossing in Fig. 1 (around 11:30 UT) would more likely correspond to > 400 minutes in the simulation time, as shown in Figs. 2b and 3a. Of course, different injections can have different temporal profiles and operate on different initial radial particle profiles, giving rise to different observations for similar satellite orbits.

Pitch angle distribution As shown in Fig. 1, the measured pitch angle distribution is slightly 'pancake'-like (slightly peaked at 90°). So even though our simulation is restricted to the magnetic equatorial plane, the simulated particles represent a significant part of the real particle distribution.

Quiet time convection electric field and corotation electric fields To date, the reported multiple discrete energy ion features [Fennell et al., 1998; Peterson et al., 1998] from Polar observations have been during quiet times following substorm activity. Our model field is definitely 'quiet' after the injection because our background field is time-independent. If the magnetic field were continuously perturbed, drift echoes would be hard to maintain and also newly injected particles (inevitable during active times) would be superimposed on previously injected particles and would make the drift echoes less distinct.

During quiet times, the convection electric field is relatively weak, on the order of 0.1mV/m, and less variable. In addition it is a potential field so that once a particle completes its drift around the Earth, the effect from the convection electric field is basically cancelled out. Both the convection and corotation electric field apply equally to all energy particles and including them should not change the main results of the simulation. However these fields will make some low energy particles stagnate or drift very slowly, so the simulated results as shown in Figs. 2 and 3 at low energies will be significantly different.

Ion Composition Figure 1 shows that the multiple band features are basically the same for different mass. Our simulation is based on the guiding center equations (1) and (2), both equations are almost mass-independent. This is consistent with the observations.

Penetrating Electric Field

Ions with energies of a few keV up to $\sim$ 20 keV are usually on open drift paths because of the global convection electric field. Depending on the strength of the convection electric field and its penetration depth into the inner magnetosphere, at a critical energy (between a few keV and 20 keV), the ions drift very slowly around the morning side instead of the evening side. Ions with energies below that critical energy would follow the convection path to the dayside magnetopause. However, during these multiple-band events, these energy ions are trapped, because they are injected deep enough into the inner magnetosphere by a deeply penetrating time-varying electric field associated with a substorm onset. During quiet times, according to the conventional convection electric field model, the electric field is shielded from in the inner magnetosphere [Maynard and Chen, 1975]. The existence of ion drift echoes even after only moderate substorm activity shows that localized time-varying electric and magnetic fields such as modeled here can and do penetrate deep into the inner magnetosphere.

Acknowledgments. We thank O. Lennartsson for discussion about TIMAS instrument, K. Trattner and A. Rakow for helping the graphic display. The work at U. of Colorado was supported by NSF/ATM-9901085 and NASA/NAG5-4896. Work at UC Berkeley was supported by NASA/NAG5-3596. Work at Lockheed Martin was supported by NASA contract NAS-3030. Work at Aerospace Corporation was supported by U. S. Air Force contract F04701-93-C-0094 plus NASA contract NAS5-30368.

References

Birn, J. et al., Substorm ion injections: Geosynchronous observations and test particle orbits in three-dimensional dynamics MHD fields, *J. Geophys. Res., 102*, 2325, 1997.

Christon, S. P., et al., Spectral characteristics of plasma sheet ion and electron populations during disturbed geomagnetic conditions, *J. Geophys. Res., 96*, 1, 1991.

Ejiri, M. et al., Energetic particle penetrations into the inner magnetosphere, *J. Geophys. Res., 85*, 653, 1980.

Fennell, J. F. et al., Multiple Discrete-Energy Ion Features in the Inner Magnetosphere: Polar Observations, *Physics of Space Plasmas*, No. 14, 395, 1998.

Grande, M. et al., Composition Signatures of Substorm Injections, Proc. of ICS-1, Kiruna, Sweden, 485, 1992.

Li, X., D. N. Baker, M. Temerin, G. Reeves, and R. Belian, Dispersionless Injection Simulations Explore Auroral Substorm Origins, *EOS*, AGU, page 405, Sept. 7, 1999.

Li, X., D. N. Baker, M. Temerin, G. Reeves, and R. Belian, Simulation of Dispersionless Injections and Drift Echoes of Energetic Electrons Associated with Substorms, *Geophys. Res. Lett., 25*, 3763, 1998.

Li, X., I. Roth, M. Temerin, J. Wygant, M. K. Hudson, and J. B. Blake, Simulation of the prompt energization and transport of radiation particles during the March 23, 1991 SSC, *Geophys. Res. Lett., 20*, 2423, 1993

Maynard, N. C., and J. J. Chen, Isol ated cold plasma region: Observations and their relation to possible production mechanisms, *J. Geophys. Res., 80*, 1009, 1975.

McIlwain, C. E., Substorm injection boundaries, *Magnetospheric Physics*, edited by B. M. McCormac, p. 143, D. Reidel, Hingham, Mass., 1974.

Mauk, B. H., and C.-I. Meng, Dynamical Injections as the Source of Near Geostationary Quiet Time Particle Spatial Boundaries, *J. Geophys. Res., 88*, 10011, 1983.

Mauk, B. H., and C.-I. Meng, Plasma injection during substorms, *Physica Scripta, T18*, 128, 1987.

Moore, T. E. et al., Propagating substorm injection fronts, *J. Geophys. Res., 86*, 6713, 1981.

Northrop, T. G., The adiabatic motion of charged particles. Interscience Publishers, New York, 1963.

Peterson, W. K. et al., Imaging the Plasma Sheet with Energetic Ions From the Polar Satellite, Proc. of ICS-4, Terra Sci. Publishing, Tokyo, 813, 1998.

Shelley, E., et al., The toroidal imaging mass-angle spectrograph (TIMAS) for the Polar mission, *Spa. Sci. Rev., 71*, 1995.

Vasyliunas, D. J., A survey of low-energy electrons in the evening sector of the magnetosphere with OGO 1 and OGO 3, *J. Geophys. Res., 73*, 2839, 1968.

Wilken, B. et al., *J. Spacecraft and Rockets, 29*, 585, 1992.

LABORATORY OPERATIONS

The Aerospace Corporation functions as an "architect-engineer" for national security programs, specializing in advanced military space systems. The Corporation's Laboratory Operations supports the effective and timely development and operation of national security systems through scientific research and the application of advanced technology. Vital to the success of the Corporation is the technical staff's wide-ranging expertise and its ability to stay abreast of new technological developments and program support issues associated with rapidly evolving space systems. Contributing capabilities are provided by these individual organizations:

Electronics and Photonics Laboratory: Microelectronics, VLSI reliability, failure analysis, solid-state device physics, compound semiconductors, radiation effects, infrared and CCD detector devices, data storage and display technologies; lasers and electro-optics, solid state laser design, micro-optics, optical communications, and fiber optic sensors; atomic frequency standards, applied laser spectroscopy, laser chemistry, atmospheric propagation and beam control, LIDAR/LADAR remote sensing; solar cell and array testing and evaluation, battery electrochemistry, battery testing and evaluation.

Space Materials Laboratory: Evaluation and characterizations of new materials and processing techniques: metals, alloys, ceramics, polymers, thin films, and composites; development of advanced deposition processes; nondestructive evaluation, component failure analysis and reliability; structural mechanics, fracture mechanics, and stress corrosion; analysis and evaluation of materials at cryogenic and elevated temperatures; launch vehicle fluid mechanics, heat transfer and flight dynamics; aerothermodynamics; chemical and electric propulsion; environmental chemistry; combustion processes; space environment effects on materials, hardening and vulnerability assessment; contamination, thermal and structural control; lubrication and surface phenomena.

Space Science Application Laboratory: Magnetospheric, auroral and cosmic ray physics, wave-particle interactions, magnetospheric plasma waves; atmospheric and ionospheric physics, density and composition of the upper atmosphere, remote sensing using atmospheric radiation; solar physics, infrared astronomy, infrared signature analysis; infrared surveillance, imaging, remote sensing, and hyperspectral imaging; effects of solar activity, magnetic storms and nuclear explosions on the Earth's atmosphere, ionosphere and magnetosphere; effects of electromagnetic and particulate radiations on space systems; space instrumentation, design fabrication and test; environmental chemistry, trace detection; atmospheric chemical reactions, atmospheric optics, light scattering, state-specific chemical reactions and radiative signatures of missile plumes.

Center for Microtechnology: Microelectromechanical systems (MEMS) for space applications; assessment of microtechnology space applications; laser micromachining; laser-surface physical and chemical interactions; micropropulsion; micro- and nanosatellite mission analysis; intelligent microinstruments for monitoring space and launch system environments.

Office of Spectral Applications: Multispectral and hyperspectral sensor development; data analysis and algorithm development; applications of multispectral and hyperspectral imagery to defense, civil space, commercial, and environmental missions.